Constraining the photon-axion coupling constant with magnetic white dwarfs

Ramandeep Gill and Jeremy S. Heyl

Phys. Rev. D **84**, 085001 — Published 4 October 2011

DOI: 10.1103/PhysRevD.84.085001

Constraining the photon-axion coupling constant with magnetic white dwarfs

Ramandeep Gill* and Jeremy S. Heyl†
Department of Physics and Astronomy, University of British Columbia
6224 Agricultural Road, Vancouver, BC V6T 1Z1, Canada

The light pseudoscalar particle, dubbed the axion, borne out of the Peccei-Quinn solution to the strong CP problem in QCD remains elusive. One avenue of inferring its existence is through its coupling to electromagnetic radiation. So far, laboratory experiments have dedicated all efforts to detect the axion in the mass range $10^{-6} < m_a < 10^{-3}$ eV with a photon-axion coupling strength $g_{a\gamma\gamma} < 10^{-10}$ GeV^{-1}, where the limits are derived from astrophysical considerations. In this study, we present a novel way of constraining $g_{a\gamma\gamma}$ by looking at the level of linear polarization in the radiation emerging from magnetic white dwarfs (mWDs). We find that photon-axion oscillations in WD magnetospheres can enhance the degree of linear polarization. Observing that most mWDs show only 5% linear polarization, we derive upper limits on $g_{a\gamma\gamma}$ for different axion masses.

PACS numbers: 14.80.Va, 97.20.Rp

I. INTRODUCTION

Quantum chromodynamics (QCD) has emerged as a phenomenologically accurate theory that describes strong interactions among the six quark flavors that are bound into two families of hadrons, namely mesons and baryons. From experiments, we understand that strong interactions enjoy C (charge conjugation), P (parity), T (time reversal) discrete symmetries of nature. Therefore, QCD must also obey such symmetries, both separately and any combinations formed thereof [1]. However, CP symmetry is broken in QCD due to the presence of the following term in the QCD Lagrangian [2]

$$\mathfrak{L}_{\rm int} = \left(\frac{\theta g^2}{32\pi^2}\right) {\rm tr}\ G_a^{\mu\nu}\tilde{G}_{a\mu\nu} \tag{1}$$

where θ is a periodic parameter, g is the QCD coupling constant, $G_{\mu\nu}$ is the color field strength tensor, and $\tilde{G}_{\mu\nu}$ is its dual. The value of the θ-parameter is not set theoretically, but it can be measured from the electric dipole moment of the neutron (d_n), for which many theoretical estimates exist but we only quote one, $\|d_n\| \sim 2.7\times10^{-16}\bar{\theta}e$ cm [3]. Here $\bar{\theta} = \theta + \arg\det m_q$, where m_q is the quark mass matrix. The latest experimental estimate of $\|d_n\| < 2.9\times10^{-26}e$ cm [4] constrains $\|\bar{\theta}\| \lesssim 10^{-11}$ [1]. This inexplicably small value of $\bar{\theta}$ gave rise to the *strong CP problem.* One of the solutions, also the most favoured, to this problem was envisioned by Peccei & Quinn [5], whereby the $\bar{\theta}$ parameter is driven precisely to zero under a global chiral symmetry, later named $U(1)_{\rm PQ}$. The pseudo-Nambu-Goldstone boson that results upon the spontaneous breakdown of this symmetry was dubbed the axion [2, 6]. Not unlike the Higgs boson, the axion has proven to be extremely difficult to observe as it couples only weakly to ordinary matter and radiation.

Despite several attempts to experimentally observe the axion, it remains elusive to this day. Nevertheless, the experimental efforts have not gone in vain, but have been able to place serious constraints on the coupling strength of the axion to photons $g_{a\gamma\gamma} < 10^{-10}$ GeV^{-1}. Stringent constraints have been placed on the mass of the axion $10^{-6} \lesssim m_a \lesssim 10^{-3}$ eV with the lower limit arising from cosmology [7] and the upper limit[1] from the neutrino flux recorded for SN 1987A, which placed strong limits on the cooling flux through other channels namely, right-handed neutrinos or axions [10]. If $g_{a\gamma\gamma} > 10^{-10}$ GeV^{-1}, the production of axions through the Primakoff process will significantly alter the core He burning timescales of post main sequence stars, a possibility excluded by the ratio of horizontal branch stars in globular clusters [11]. Several reviews on the properties of axions have been forthcoming in the past decade, for example see [1, 12, 13], to which we point the reader for a more detailed and comprehensive exposition.

Still, there is no denying the fact that none of the laboratory experiments conducted thus far have been able to secure a positive detection of this mysterious particle. The detection of very weakly coupled particles demands extremely sensitive laboratory experiments. So far, only a handful of experiments, namely the Cern Axion Solar Telescope (CAST) [14], Axion Dark Matter Experiment (ADMX) [15, 16], and Rochester-Brookhaven-Fermilab (RBF) collaboration [17, 18] have been able to surpass the astrophysically derived limits on $g_{a\gamma\gamma}$ in the above quoted axion mass range. Yet, the sensitivity envelope needs to be pushed even further by a few orders of magitude to be able to draw any definitive conclusions about the existence of the axion. Plans are afoot to modifiy the existing experiments and devise new ones to improve upon current limits on $g_{a\gamma\gamma}$ (see Section IV).

* rsgill@phas.ubc.ca
† heyl@phas.ubc.ca

[1] Due to large uncertainties in the axion mass derived for the DFSZ model [8, 9] from SN 1987A observations ($0.004 \lesssim m_a \lesssim 0.012$ eV), a more relaxed upper limit is $m_a \lesssim 0.01$ eV [10]

Unlike the laboratory experiments, the odds are in favour for detecting axions in astrophysical systems. This optimism stems from the fact that the axion to photon conversion probability scales with large magnetic field strengths and longer coherence lengths [19], such that $P_{a\to\gamma} \propto g^2 B^2 L^2$, where L is the length over which both the photon and axion fields are in phase. Thus, there is a very good chance of finding the axion in strongly magnetized compact objects, namely magnetic white dwarfs (mWDs) and neutron stars (NSs). The possibility in the latter case has been expounded by many (see for example [19–22]; also see [23] where constraints on $g_{a\gamma\gamma}$ are derived from the dimming of radiation by photon-axion conversion in astrophysical sources), however, the case of the mWDs has not been investigated in great detail and warrants further study.

A. Magnetic white dwarfs

After the discovery of the first mWD by Kemp [24], the number of white dwarfs with magnetic fields ranging from a few kG to 10^3 MG has grown to about 170. The size of this subpopulation is only 3% of the total population of known WDs comprising of 5447 objects[2]. The main channel for identifying magnetism in WDs is through Zeeman spectropolarimetry, which not only allows one to discern the strength of the field but also the direction of the field lines, and also through cyclotron spectroscopy (see for e.g. [25] for a review on isolated and binary mWDs). Nevertheless, reconstruction of the field topology has proven to be very difficult, mainly due to its highly non-dipolar structure. Over the last decade Zeeman tomography of mWDs has enjoyed some success in elucidating the underlying field structure. This technique is based on calculating a database of model spectra, where different field geometries comprising of single/multiple dipole, and higher multipoles, that may also be off-centered and misaligned with the rotational axis, are considered. Then a least-squares fit using the pre-calculated synthetic spectra is performed through a highly optimized algorithm on the phase-resolved Zeeman spectra to obtain the complex field structures [26]. The generality of the models not only allows greater flexibility but also renders a closer fit to the actual field geometry of the source for a given rotational phase.

The presence of even a small degree of circular polarization in the spectrum of a WD is a strong indicator of the object possessing a magnetic field upwards of 10^6 G [27]. The degree of circular polarization typically reaches up to $\sim 5\%$, and sometimes beyond that in a few selective objects, near absorption features and also in the continuum. Continuum circular polarization stems from the magnetic circular dichroism of the atmosphere, where the left and right circularly polarized waves propagating through a magnetized medium encounter unequal opacities [28]. A relatively higher degree of circular polarization also appears near the red and blue shifted wings of the Zeeman split absorption lines (σ_+ and σ_- components, [25]).

On the other hand, most observations of mWDs indicate that the linear polarization component never exceeds that of the circular one, and the spectrum remains dominantly circularly polarized until field strengths $\geq 10^8$ G are reached [28]. In a magneto-active plasma, the plane of linear polarization undergoes many Faraday rotations, an effect that arises due to the magnetic birefringence of the medium, so that on average the degree of linear polarization of the emergent radiation is much reduced [29].

The very fact that linear polarization is of the order of a few percent ($\sim 5\%$) in the continuum spectra of most mWDs can be exploited to draw meaningful conclusions on the extent of axion interaction with photons traversing the magnetized plasma of mWDs. We explain how this can be implemented in the next section.

B. Plan of this study

The purpose of this study is to conduct a survey of the $m_a - g_{a\gamma\gamma}$ parameter space by modelling photon-axion oscillations in the magnetosphere of a mWD. To this end, we model the field structure of a strongly magnetized WD PG 1015+014, for which high resolution optical spectropolarimetric observations are available [30]. In the same article, the authors also conduct a phase-resolved Zeeman tomographic analysis and derive a best-fit model of the magnetic field topology. Despite fitting the spectrum with a range of field geometries, they were only able to pin down the field geometry for a single rotational phase by fitting it with a superposition of three off-centered and non-aligned dipoles of unequal surface field strengths (see Table I for model parameters). To model the effect of photon-axion oscillation in the magnetosphere on the emergent polarization, we propagate an unpolarized photon of a given energy from the photosphere through the encompassing magnetosphere, that has been populated by a diffuse, cold ionized H gas. The emergent intensity and polarization is then averaged over the whole surface of the star. Finally, we compare the degree of polarization from our model simulation to what is observed in mWDs with field strengths in excess of a few 10^6 G, for example PG 1015+014, and draw conclusions on the strength of the coupling constant for a given axion mass.

In the following Section, we formulate the key equations describing the interaction of the axion with photons, geometry of the aggregate magnetic field, and structure of the plasma permeating the magnetosphere. The lack of understanding of the density profile of the magne-

[2] G.P. McCook and E.M. Sion, web version of the Villanova White Dwarf Catalog, http://www.astronomy.villanova.edu/WDCatalog/index.html

TABLE I. *Top*: Magnetic field geometry adopted from the spectropolarimetric analysis by [30] of the the mWD PG 1015+014. The model comprises of three off-centered and non-aligned dipoles D_1, D_2, D_3 with unequal surface field strengths B_s, polar (θ_B) and azimuthal (ϕ_B) angles of the magnetic field axes. The center positions of the dipoles relative to the center of the star are given by (a_x, a_y, a_z). *Bottom*: Collection of parameters used in the study.

Model Parameters

	D_1	D_2	D_3
B_s (MG)	-40	92	-38
$\theta_B(^\circ)$	44	63	63
$\phi_B(^\circ)$	339	276	134
$a_x(R_\star)$	0.04	-0.012	0.27
$a_y(R_\star)$	0.35	-0.136	0.080
$a_z(R_\star)$	0.33	-0.28	0.21
$R_\star$			7×10^8 cm
θ_k			23°
Y_e			1
B_Q			4.413×10^{13} G
T			10^4 K
$g_\star$			10^8 cm s^{-2}
ρ_0			10^{-10} g cm^{-3}
ρ_∞			10^{-20} g cm^{-3}

tospheric plasma introduces some level of inaccuracy in any treatment of mWDs. We take the simplest approach and describe the plasma density by the barometric law for an isothermal atmosphere. In Section III we present the main results of the study along with a comparison to some of the results obtained from lab experiments (see Fig. 5). A discussion of the results is provided in Section IV.

II. MODEL EQUATIONS

The interaction of the axion field with an external electromagnetic field is given by the following Lagrangian density [20], in natural units where $\hbar = c = 1$,

$$\mathfrak{L} = -\tfrac{1}{4}F_{\mu\nu}F^{\mu\nu} + \tfrac{1}{2}(\partial_\mu a \partial^\mu a - m_a^2 a^2) - \tfrac{1}{4}g_{a\gamma\gamma}F_{\mu\nu}\tilde{F}^{\mu\nu}a + \tfrac{\alpha^2}{90 m_e^4}\left[(F_{\mu\nu}F^{\mu\nu})^2 + \tfrac{7}{4}\left(F_{\mu\nu}\tilde{F}^{\mu\nu}\right)^2\right] \qquad (2)$$

where the first term describes the external electromagnetic field, with $F_{\mu\nu}$ as the antisymmetric electromagnetic field strength tensor and $\tilde{F}^{\mu\nu} = \frac{1}{2}\varepsilon^{\mu\nu\rho\sigma}F_{\rho\sigma}$ as its dual. The second term is simply the Klein-Gordon equation for the axion field a where m_a represents its mass. The next term is the interaction Lagrangian density, which upon simplification, using the given definitions, yields $\mathfrak{L}_{\text{int}} = g_{a\gamma\gamma} a \mathbf{E}\cdot\mathbf{B}$, where $g_{a\gamma\gamma}$ is the photon-axion coupling strength, $\mathbf{E}$ is the polarization vector of the photon field, and $\mathbf{B}$ is the external magnetic field. Quantum corrections to the classical electromagnetic field, due

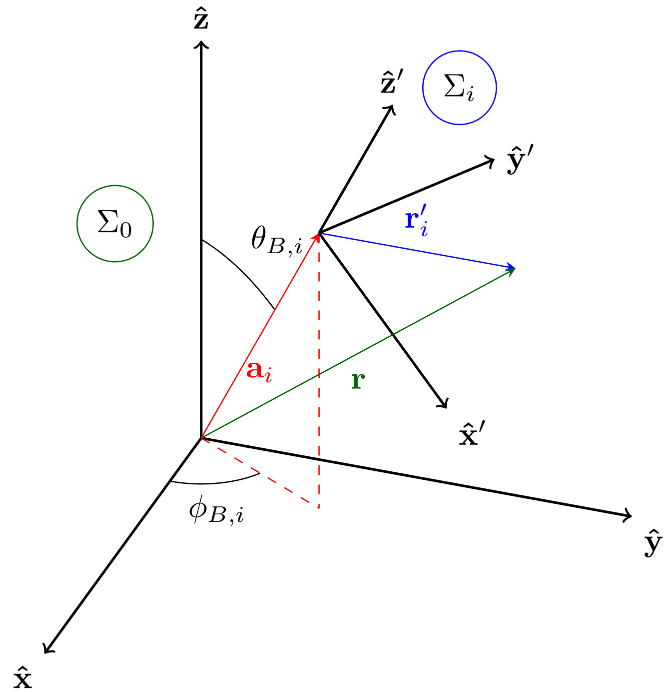

FIG. 1. This illustrates the coordinate system used to obtain the aggregate magnetic field. Here Σ_0 represents the coordinate system centered on the star with the $\hat{\mathbf{z}}$-axis aligned with the rotational axis. Σ_i represents the coordinate system in which the different dipole magnetic field equations are written. This system is misaligned with Σ_0 by a polar angle $\theta_{B,i}$ and an azimuthal angle $\phi_{B,i}$, and then it is displaced from the center by the vector $\mathbf{a}_i$. For clarity we have chosen the vector $\mathbf{a}_i$ to lie along the $\hat{\mathbf{z}}'$-axis (color online).

to the constant creation and annihilation of electron-positron pairs in vacuum, are given in the last term of (2) by the Euler-Heisenberg effective Lagrangian, causing the vacuum to be birefringent.

A. Off-centered non-aligned three dipole model

We start by writing down the aggregate magnetic field $\mathbf{B}_0$ in the coordinate system Σ_0 where the $\hat{\mathbf{z}}$-axis coincides with the rotational axis of the star

$$\mathbf{B}_0 = \sum_{i=1}^{3} R_i^T \mathbf{B}_i' \qquad (3)$$

The three off-centered dipole fields $\mathbf{B}_i'$ are first rotated before they are added together by operating on each of them with a rotation matrix $R^T = R_{z,i}^T R_{y,i}^T$, where the superscript T indicates the transpose, and the rotation matrices are given as follows

$$R_{z,i} = \begin{pmatrix} \cos\phi_{B,i} & \sin\phi_{B,i} & 0 \\ -\sin\phi_{B,i} & \cos\phi_{B,i} & 0 \\ 0 & 0 & 1 \end{pmatrix} \qquad (4)$$

$$R_{y,i} = \begin{pmatrix} \cos\theta_{B,i} & 0 & -\sin\theta_{B,i} \\ 0 & 1 & 0 \\ \sin\theta_{B,i} & 0 & \cos\theta_{B,i} \end{pmatrix} \tag{5}$$

Here the polar and azimuthal angles $\theta_{B,i}$ and $\phi_{B,i}$, respectively, are defined with respect to the axis of rotation. In cartesian coordinates, the dipole fields are expressed as

$$\mathbf{B}'_i = \frac{B_{s,i}R_\star^3}{2r_i'^5}(3x'_iz'_i\hat{\mathbf{x}}' + 3y'_iz'_i\hat{\mathbf{y}}' + \{3z_i'^2 - r_i'^2\}\hat{\mathbf{z}}') \tag{6}$$

where the fields are shifted from the coordinate center, such that $\mathbf{r}'_i = \mathbf{r} - \mathbf{a}_i$. In the above equation, $\mathbf{B}_{s,i}$ is the surface field strength of the i^{th} dipole field component, $R_\star \simeq 7\times10^8$ cm is the radius of the WD, and r'_i is the magnitude of the radial vector in the coordinate system Σ_i. The profile of the aggregate field B_0 as a function of distance is shown in Fig. 2.

B. Fully ionized pure H atmosphere

The presence of a magnetic field necessarily introduces anisotropy in the plasma dielectric tensor $\underline{\underline{\varepsilon}}_p$. In the case of a nonuniform field, none of the dielectric tensor components vanish, as compared to the homogeneous case. Below we write all the dielectric components, which one can easily derive from Maxwell's equations, for completeness.

$$\underline{\underline{\varepsilon}}_p = \begin{pmatrix} \varepsilon_{11} & \varepsilon_{12} & \varepsilon_{13} \\ \varepsilon_{21} & \varepsilon_{22} & \varepsilon_{23} \\ \varepsilon_{31} & \varepsilon_{32} & \varepsilon_{33} \end{pmatrix} \tag{7}$$

$$\varepsilon_{11} = 1 - \sum_{s=e,p}\hat{\omega}_{p,s}^2\left[\frac{1-\hat{\omega}_{c,s}^2\hat{B}_{0x}^2}{1-\hat{\omega}_{c,s}^2}\right]$$

$$\approx 1 - \hat{\omega}_{p,e}^2\left[\frac{1-\hat{\omega}_{c,e}^2(1+\hat{\omega}_{c,p}^2)\hat{B}_{0x}^2}{(1-\hat{\omega}_{c,e}^2)(1-\hat{\omega}_{c,p}^2)}\right] \tag{8}$$

$$\varepsilon_{12} \approx \frac{\hat{\omega}_{c,e}\hat{\omega}_{p,e}^2}{(1-\hat{\omega}_{c,e}^2)}(i\hat{B}_{0z} + \hat{\omega}_{c,e}\hat{B}_{0x}\hat{B}_{0y}) \tag{9}$$

$$\varepsilon_{13} \approx -\frac{\hat{\omega}_{c,e}\hat{\omega}_{p,e}^2}{(1-\hat{\omega}_{c,e}^2)}(i\hat{B}_{0y} - \hat{\omega}_{c,e}\hat{B}_{0x}\hat{B}_{0z}) \tag{10}$$

$$\varepsilon_{21} \approx -\frac{\hat{\omega}_{c,e}\hat{\omega}_{p,e}^2}{(1-\hat{\omega}_{c,e}^2)}(i\hat{B}_{0z} - \hat{\omega}_{c,e}\hat{B}_{0x}\hat{B}_{0y}) \tag{11}$$

$$\varepsilon_{22} \approx 1 - \hat{\omega}_{p,e}^2\left[\frac{1-\hat{\omega}_{c,e}^2(1+\hat{\omega}_{c,p}^2)\hat{B}_{0y}^2}{(1-\hat{\omega}_{c,e}^2)(1-\hat{\omega}_{c,p}^2)}\right] \tag{12}$$

$$\varepsilon_{23} \approx \frac{\hat{\omega}_{c,e}\hat{\omega}_{p,e}^2}{(1-\hat{\omega}_{c,e}^2)}(i\hat{B}_{0x} + \hat{\omega}_{c,e}\hat{B}_{0y}\hat{B}_{0z}) \tag{13}$$

$$\varepsilon_{31} \approx \frac{\hat{\omega}_{c,e}\hat{\omega}_{p,e}^2}{(1-\hat{\omega}_{c,e}^2)}(i\hat{B}_{0y} + \hat{\omega}_{c,e}\hat{B}_{0x}\hat{B}_{0z}) \tag{14}$$

$$\varepsilon_{32} \approx -\frac{\hat{\omega}_{c,e}\hat{\omega}_{p,e}^2}{(1-\hat{\omega}_{c,e}^2)}(i\hat{B}_{0x} - \hat{\omega}_{c,e}\hat{B}_{0y}\hat{B}_{0z}) \tag{15}$$

$$\varepsilon_{22} \approx 1 - \hat{\omega}_{p,e}^2\left[\frac{1-\hat{\omega}_{c,e}^2(1+\hat{\omega}_{c,p}^2)\hat{B}_{0z}^2}{(1-\hat{\omega}_{c,e}^2)(1-\hat{\omega}_{c,p}^2)}\right] \tag{16}$$

In the above set of equations, $\hat{\omega}_{c,s} = q_sB_0/\omega m_sc$ is the normalized cyclotron frequency for species $s = (e,p)$, where e and p signify electrons and protons; $\hat{\omega}_{p,s} = \sqrt{4\pi n_s/m_s\omega^2}$ is the normalized plasma frequency, where $n_p = n_e = Y_e\rho/m_p$ are the electron and proton number densities, Y_e is the electron fraction, and ρ is the proton mass density of the plasma; the normalized magnetic field components are defined as $\hat{B}_{0,i=x,y,z} = B_{0,i}/B_0$.

1. Vacuum corrections

Due to the polarizability of the vacuum in strong magnetic fields, the plasma dielectric tensor $\underline{\underline{\varepsilon}}_p$, and the inverse permeability tensor $\underline{\underline{\mu}}^{-1}$ are modified [31, 32], such that $\underline{\underline{\varepsilon}}_{p+v} = \underline{\underline{\tilde{\varepsilon}}} = \underline{\underline{\varepsilon}}_p + \Delta\underline{\underline{\varepsilon}}_v$ and $\underline{\underline{\mu}}^{-1}_{p+v} = \underline{\underline{\tilde{\mu}}}^{-1} = \underline{\underline{I}} + \Delta\underline{\underline{\mu}}^{-1}_v$, where

$$\Delta\underline{\underline{\varepsilon}}_v = (a_v - 1)\underline{\underline{I}} + q_v\hat{\mathbf{B}}_0\hat{\mathbf{B}}_0 \tag{17}$$

$$\Delta\underline{\underline{\mu}}^{-1}_v = (a_v - 1)\underline{\underline{I}} + m_v\hat{\mathbf{B}}_0\hat{\mathbf{B}}_0 \tag{18}$$

$$a_v = 1 - 2\delta_v \quad q_v = 7\delta_v \quad m_v = -4\delta_v \quad \delta_v = \frac{\alpha}{45\pi}\left(\frac{B_0}{B_Q}\right)^2$$

and $B_Q = 4.413\times10^{13}$ G is the quantum critical field for which the separation in energy between Landau levels of the electron exceeds its rest mass.

2. Plasma density profile

That many mWDs are surrounded by hot coronae has been suggested by many to explain the polarized flux of those WDs that show comparable degree of linear and circular polarization [29, 33, 34]. The thermal electrons in the hot tenuous plasma with temperature $T \sim 10^{6-8}$ K radiate at the cyclotron frequency that falls in the optical wavelength for field strengths of $B \sim 10^8$ G. This radiation appears to be polarized both linearly and circularly, depending on the orientation of the line of sight to the magnetic field, and traverses the corona without any absorption. Furthermore, slightly polarized radiation emanating from the photosphere, with very low degree of linear polarization due to Faraday rotation, gets added to that generated in the corona, as a result increasing the amount of flux that is polarized linearly. Several hot isolated WDs, with effective temperatures in excess of $\simeq 25,000$ K, emitting X-rays were detected by ROSAT [35], however all cases were linked to subphotospheric thermal emission [36]. Although the non-detection of any coronal emission may indicate the absence of a hot tenuous corona, it is not at all unreasonable to suggest the presence of a tenuous cold plasma of fully ionized H. In this study, we envisage that the mWDs are encompassed by cold isothermal electron-proton coronae with the following barometric density profile,

$$\rho(r) = \rho_0 \exp\left(-\frac{r - R_\star}{H_\rho}\right) + \rho_\infty \tag{19}$$

where ρ_0 is the density near the surface of the star, ρ_∞ is the density that remains far away from the star as the strength of the magnetic field becomes significantly weaker than that at the surface, and $H_\rho = 2k_B T/m_p g_\star \simeq 1.65 \times 10^4$ cm is the density scale height with an effective temperature $T \simeq 10^4$ K and surface gravity $\log g_\star(\mathrm{cm/s}^2) = 8$. There is no clear agreement on the surface plasma density with $10^{-11} \lesssim \rho_0 \lesssim 10^{-6}$ g cm^{-3}. Here, we assume that the plasma is sufficiently tenuous with $\rho_0 = 10^{-10}$ g cm^{-3} and $\rho_\infty = 10^{-20}$ g cm^{-3}.

C. Axion-photon mode evolution in an inhomogeneous magnetized plasma

We are interested in knowing the evolution of the axion field and the polarization vector as the radiation propagates out from the surface of the star, traversing the region with an inhomogeneous plasma density and magnetic field. Here we follow the discussion given in [20, 21], and derive the photon field mode evolution from the EM wave equation

$$\nabla \times (\underline{\underline{\mu}}^{-1} \cdot \nabla \times \mathbf{E}) = \frac{\omega^2}{c^2} \underline{\underline{\varepsilon}} \cdot \mathbf{E} \tag{20}$$

Next, we assume the ansatz $\mathbf{E} = \tilde{\mathbf{E}} \exp(ikz)$ where the wave is propagating along the rotational axis of the star, which in this case is also the line of sight direction, and the wavenumber $k = \omega/c$. Plugging this ansatz into the wave equation, and ignoring second order derivatives, we find

$$\frac{d}{dz}\begin{pmatrix} \tilde{E}_x \\ \tilde{E}_y \end{pmatrix} = \begin{pmatrix} \chi_{11} & \chi_{12} \\ \chi_{21} & \chi_{22} \end{pmatrix}\begin{pmatrix} \tilde{E}_x \\ \tilde{E}_y \end{pmatrix} \tag{21}$$

where the matrix elements are given below

$$\chi_{11} = \Upsilon_3^{-1}\left[k^2\tilde{\varepsilon}_{11} - \Upsilon_4 - \left(1 - \frac{\Upsilon_1^2}{\Upsilon_3\Upsilon_5}\right)^{-1}\Upsilon_1\Upsilon_5^{-1} \times \left(k^2\tilde{\varepsilon}_{21} - \Upsilon_2 - \frac{\Upsilon_1}{\Upsilon_3}\{k^2\tilde{\varepsilon}_{11} - \Upsilon_4\}\right)\right] \tag{22}$$

$$\chi_{12} = \Upsilon_3^{-1}\left[k^2\tilde{\varepsilon}_{12} - \Upsilon_2 - \left(1 - \frac{\Upsilon_1^2}{\Upsilon_3\Upsilon_5}\right)^{-1}\Upsilon_1\Upsilon_5^{-1} \times \left(k^2\tilde{\varepsilon}_{22} - \Upsilon_6 - \frac{\Upsilon_1}{\Upsilon_3}\{k^2\tilde{\varepsilon}_{12} - \Upsilon_2\}\right)\right] \tag{23}$$

$$\chi_{21} = \left(1 - \frac{\Upsilon_1^2}{\Upsilon_3\Upsilon_5}\right)^{-1}\Upsilon_5^{-1} \times \left(k^2\tilde{\varepsilon}_{21} - \Upsilon_2 - \frac{\Upsilon_1}{\Upsilon_3}\{k^2\tilde{\varepsilon}_{11} - \Upsilon_4\}\right) \tag{24}$$

$$\chi_{22} = \left(1 - \frac{\Upsilon_1^2}{\Upsilon_3\Upsilon_5}\right)^{-1}\Upsilon_5^{-1} \times \left(k^2\tilde{\varepsilon}_{22} - \Upsilon_6 - \frac{\Upsilon_1}{\Upsilon_3}\{k^2\tilde{\varepsilon}_{12} - \Upsilon_2\}\right) \tag{25}$$

$$\Upsilon_1 = \frac{d}{dz}(m_v\hat{B}_x\hat{B}_y) + i2km_v\hat{B}_x\hat{B}_y \tag{26}$$

$$\Upsilon_2 = ik\frac{d}{dz}(m_v\hat{B}_x\hat{B}_y) - k^2m_v\hat{B}_x\hat{B}_y \tag{27}$$

$$\Upsilon_3 = -\frac{d}{dz}(a_v + m_v\hat{B}_y^2) + i2k(a_v + m_v\hat{B}_y^2) \tag{28}$$

$$\Upsilon_4 = -ik\frac{d}{dz}(a_v + m_v\hat{B}_y^2) + k^2(a_v + m_v\hat{B}_y^2) \tag{29}$$

$$\Upsilon_5 = -\frac{d}{dz}(a_v + m_v\hat{B}_x^2) + i2k(a_v + m_v\hat{B}_x^2) \tag{30}$$

$$\Upsilon_6 = -ik\frac{d}{dz}(a_v + m_v\hat{B}_x^2) + k^2(a_v + m_v\hat{B}_x^2) \tag{31}$$

1. *Line of sight geometry*

The Zeeman tomography analysis of mWD PG 1015+014 indicates that the line of sight (LOS) is inclined at an angle $\theta_k = 23°$ to the rotational axis of the star. Following [37], we modify the matrix Eq.(21) to obtain the mode evolution of the photon-axion system in a coordinate system oriented along the LOS (see Fig. 2). Again, we assume the ansatz $a \propto \exp(ik's - i\omega t)$

$$i\frac{d}{ds}\begin{pmatrix} a \\ E_{x'} \\ E_{y'} \end{pmatrix} = \begin{pmatrix} \Delta_a - k' & \Delta_{Mx'} & \Delta_{My'} \\ \Delta_{Mx'} & i\chi'_{11} - k' & i\chi'_{12} \\ \Delta_{My'} & i\chi'_{21} & i\chi'_{22} - k' \end{pmatrix}\begin{pmatrix} a \\ E_{x'} \\ E_{y'} \end{pmatrix} \tag{32}$$

where $\Delta_a = m_a^2/2\omega$, $\Delta_{Mx'} = -g_{a\gamma\gamma}B_x/2$, $\Delta_{My'} = -g_{a\gamma\gamma}B_y/2$. Notice that Eq.(21) applies to a system for which the LOS vector coincides with the rotational axis of the star. For a different LOS vector, such as shown in Fig. 2, we perform a rotation of the plasma dielectric tensor around the $\hat{\mathbf{y}}$-axis by an angle θ_k, $\underline{\underline{\tilde{\varepsilon}}}' = R_y^T(\theta_k)\underline{\underline{\tilde{\varepsilon}}}R_y(\theta_k)$ where R_y is given in Eq.(5).

The total degree of polarization can be found by integrating Eq.(32) from a given point on the surface outwards to a distance beyond which the amplitude of photon-axion oscillations and plasma effects become negligible, and then by averaging the Stokes parameters [38] over the whole observable hemisphere.

$$I = \|E_{x'}\|^2 + \|E_{y'}\|^2 \tag{33}$$

$$Q = \|E_{x'}\|^2 - \|E_{y'}\|^2 \tag{34}$$

$$U = E_{x'}E_{y'}^* + E_{y'}E_{x'}^* \tag{35}$$

$$V = -i(E_{x'}E_{y'}^* - E_{y'}E_{x'}^*) \tag{36}$$

The mode amplitudes are in general complex, and in the above set of equations $*$ gives the complex conjugate. We sample the Stokes vector from different points on the surface, with coordinates $(R_\star, \theta_R, \phi_R)$, that are spread around the LOS vector $\hat{\mathbf{k}}$ with $\Delta\phi_R = 30°$ and $\Delta\theta_R = 10°$, where $10° \le \theta_R \le 80°$ and $0° \le \phi_R \le 330°$.

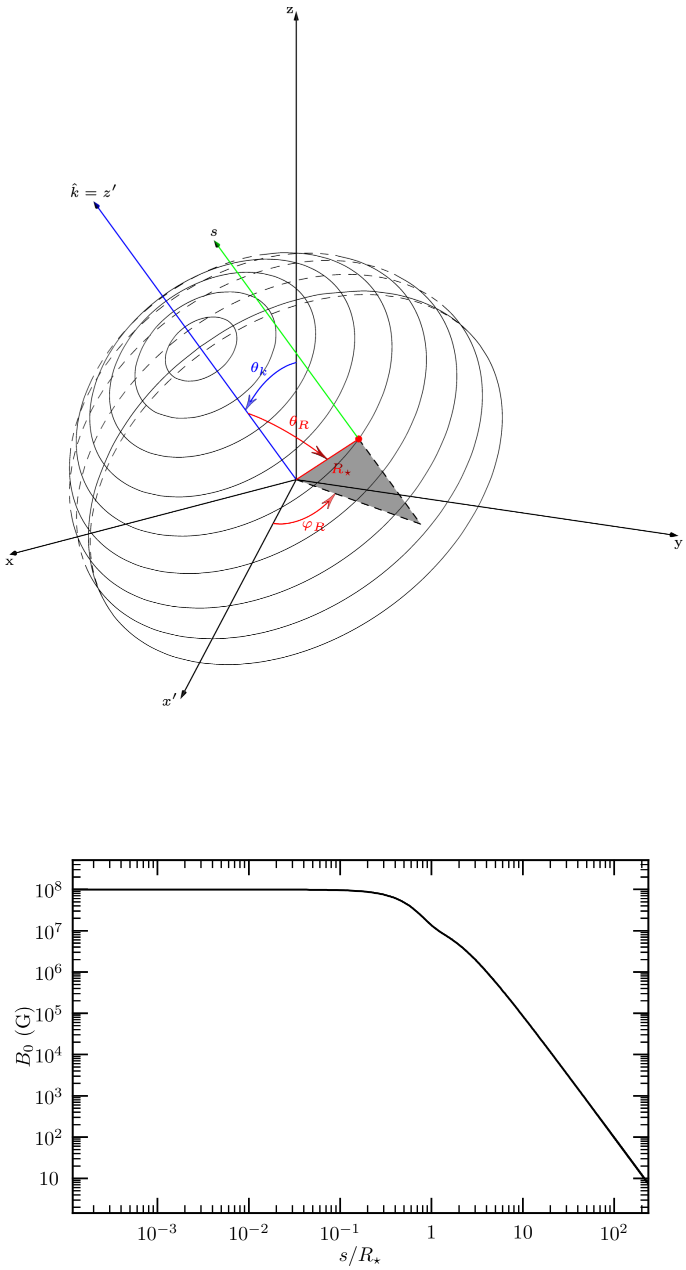

FIG. 2. This figure illustrates the coordinate system used to obtain the photon-axion mode evolution along a given LOS (top), and the decline of the magnetic field strength with distance s from the surface (bottom). Here the LOS vector is represented by s that is tilted at an angle θ_k to the rotation axis, and is in parallel to z' which is not to be confused with $\hat{z}'$ in Fig. 1. Several different points on the star's surface with spherical coordinates $(R_\star, \theta_R, \phi_R)$ are chosen and then averaged to determine the final polarization of the photon leaving the magnetosphere (color online).

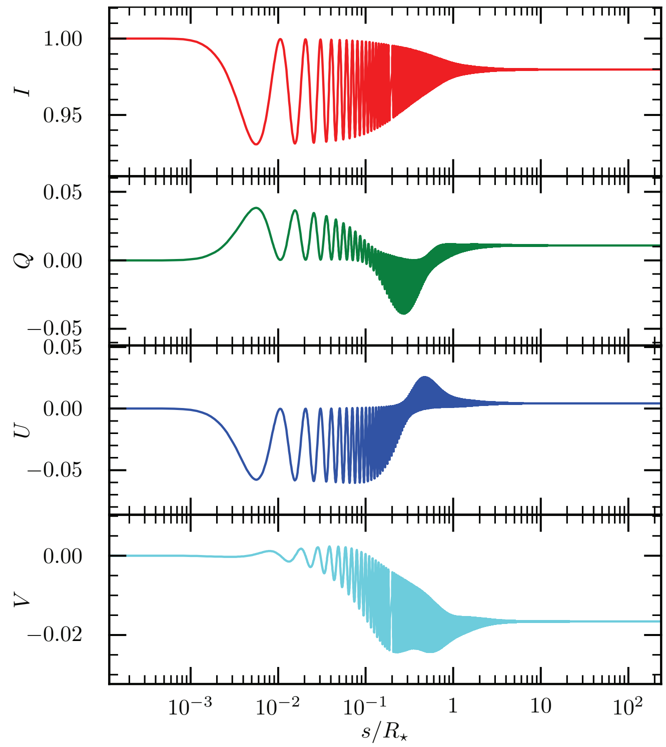

FIG. 3. Polarization evolution of an unpolarized photon along a given LOS as it starts at the photosphere and propagates through the magnetosphere. In this case, $E_\gamma = 3$ eV, $m_a = 10^{-5}$ eV, $g_{a\gamma\gamma} = 10^{-9}$ GeV^{-1}. The magnetic field geometry assumed is that of mWD PG 1015+014 (color online).

Because the sampling in the azimuthal angle is sparse for larger polar angles, we take a weighted average, as shown below for one of the Stokes parameters, to determine the average degree of polarization of the whole hemisphere

$$\langle I \rangle = \frac{\sum_{\theta_R, \phi_R} I(\theta_R, \phi_R) \sin\theta_R}{\sum_{\theta_R} \sin\theta_R} \tag{37}$$

III. RESULTS

In the following, we look at how an unpolarized photon emitted from the photosphere of a mWD gets polarized as it traverses through the magnetosphere. Photon-axion interaction and the intervening plasma make the medium birefringent, consequently, altering the state of polarization of the unpolarized photon. We obtain the degree of polarization from the averaged Stokes parameters

$$P_L = \frac{\sqrt{\langle Q \rangle^2 + \langle U \rangle^2}}{\langle I \rangle} \tag{38}$$

$$P_C = \frac{\langle V \rangle}{\langle I \rangle} \tag{39}$$

where P_L and P_C represent linear and circular polarization.

In Fig. 3, we present the evolution of the Stokes vector with distance s from the surface of the star for the case of radiation with $E_\gamma = 3$ eV, and axion parameters $m_a = 10^{-5}$ eV, $g_{a\gamma\gamma} = 10^{-9}$ GeV^{-1}. The oscillations in the solution arise due to the mixing of the axion and photon eigenstates, an effect analogous to neutrino oscillations due to the MSW effect [39, 40]. However, notice that the interaction is non-resonant because a 50% drop in intensity would be observed if the axion and photon modes were to achieve maximal mixing and undergo level crossing. Eventually, as the photons travel farther away from the surface, the decline in the magnetic field strength reduces the probability of conversion, hence the diminishing of intensity variation. We find that the change in polarization is primarily brought about by the axion interaction with the photon. In the event this interaction is made negligible, no significant polarization or change in intensity of the emergent radiation is found. The origin of circular polarization in mWDs, as alluded to earlier, is understood in terms of the difference in opacities for the two modes of radiation, making the plasma dichroic, in the presence of a magnetic field. Linear polarization, on the other hand, was explained by the cyclotron radiation that emanates from the tenuous corona composed of an ionized plasma. In this study, since the treatment of radiative transfer effects is very simplistic only an upper limit can be placed on how strongly the axion couples to photons, as shown in the next section.

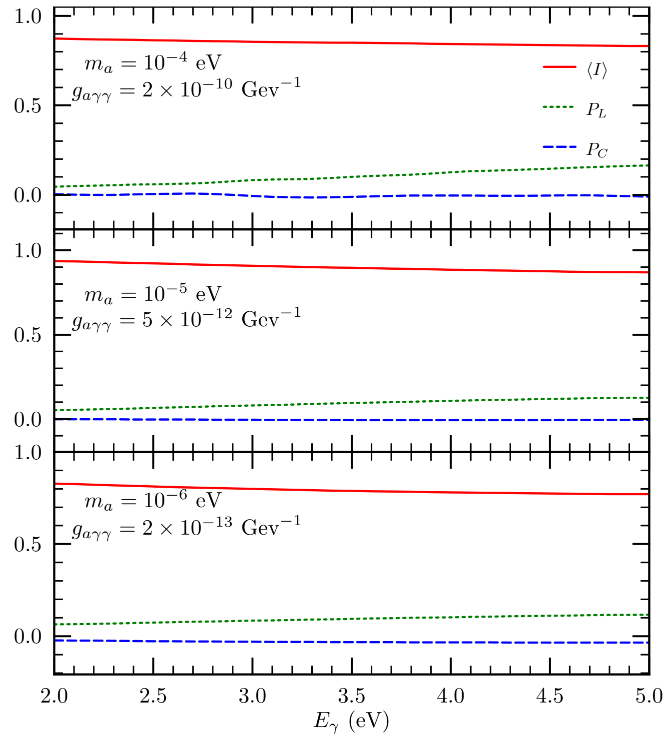

FIG. 4. The final state of polarization of radiation after traversal from the WD's magnetosphere for different m_a and $g_{a\gamma\gamma}$. Here $\langle I \rangle$ is the average Stokes intensity, and P_L and P_C are the degrees of linear and circular polarizations. These results apply to the case of mWD PG 1015+014 (color online).

A. Constraints on $g_{a\gamma\gamma}$

Axion production in the mWD magnetosphere can enhance the degree of linear polarization of the observed optical radiation. The goal here is to not determine the precise value of the photon-axion coupling strength but only constrain it from above. To this end, we look at the amount of linear polarization that is produced for a given m_a and $g_{a\gamma\gamma}$. The underlying assumption here is that all of the observed linear polarization is generated due to photon-axion interaction, and not by the plasma, which effectively yields the absolute upper limit on $g_{a\gamma\gamma}$. In Fig. 4, we plot the emergent intensity and state of polarization for different axion masses and for photons in the UV - optical waveband with energies between $2-5$ eV. The m_a and $g_{a\gamma\gamma}$ in Fig. 4 were chosen specifically so that $P_L \gtrsim 0.05$ for all photon energies.

In Fig. 5, we use the same parameters to draw an exclusion region in the $m_a - g_{a\gamma\gamma}$ parameter space, along with regions excluded by lab experiments and astrophysical considerations. The shaded region in red excludes all m_a - $g_{a\gamma\gamma}$ values for the case of mWD PG 1015+014, that is for a typical surface field strength $B \simeq 10^8$ G and degree of linear polarization $P_L \sim 5\%$. We find that for the range of masses that are of relevance, in particular, to the axion models, the constraints on $g_{a\gamma\gamma}$ from this study are superseded by that from horizontal branch (HB) stars. Still, the limiting linear polarization criterion used in this study is able to probe smaller $g_{a\gamma\gamma}$ values in comparison to works that only look at radiation dimming (for e.g. see [23]).

The constraints can be further improved by looking at mWDs with higher magnetic field strengths. The highest field strength that has ever been discovered in a mWD is $B \simeq 1000$ MG in two such objects namely, PG 1031+234 and SDSS J234605+385337 [41]. Both objects show linear polarization as low as $\sim 1\%$ for some rotational phases [42, 43]. Based on these two facts and assuming that the magnetic field geometry of these two mWDs is at least as complex as that found in PG 1015+014, we produce two exclusion regions shown in Fig. 5 with colors blue and green. The former corresponds to a surface field strength $B = 1000$ MG with the same level of linear polarization as before, and the latter studies the case with $P_L \simeq 1\%$. For these two cases, we have only looked at $m_a \leq 10^{-5}$ eV since higher mass values don't constrain $g_{a\gamma\gamma}$ better than limits derived from HB stars and CAST (Phase-I). On the other hand, we have extended our treatment to smaller particle masses with $m_\phi \leq 10^{-6}$ eV where m_ϕ should be interpreted as the mass of any light pseudoscalar boson that is characteristically very much similar to the axion but isn't a CDM particle.

It is worth mentioning that the change in $g_{a\gamma\gamma}$ is not linear with the change in magnetic field strength, as evident from the comparison between the red and blue regions in Fig. 5. For higher field strengths one observes higher degree of polarization of the emerging radiation.

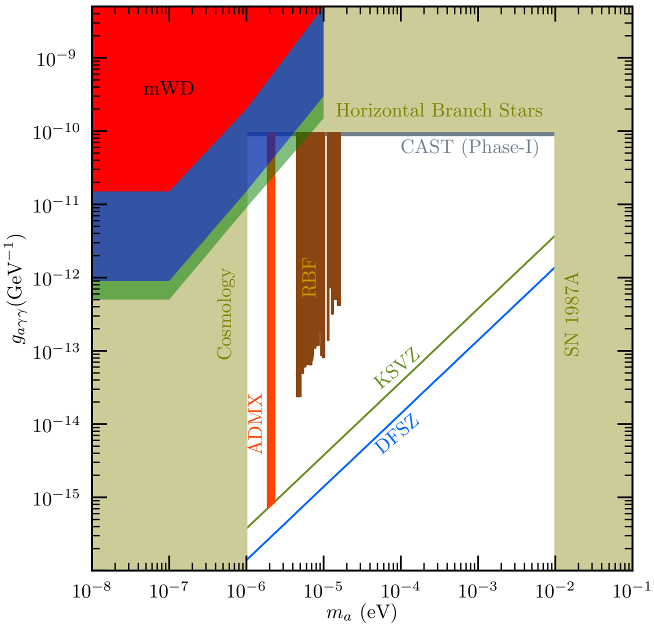

FIG. 5. Exclusion plot in the $m_a - g_{a\gamma\gamma}$ parameter space. The red region corresponds to the case of mWD PG 1015+014 with $B \simeq 10^8$ G and limiting linear polarization $P_L \sim 5\%$. The blue and green regions correspond to the case with $B \simeq 10^9$ G, but with $P_L \sim 5\%$ and $P_L \sim 1\%$ respectively. The mass of the axion is constrained to $10^{-6} \lesssim m_a \lesssim 10^{-2}$ eV from cosmology and SN 1987A measurments. The photon-axion coupling constant is capped from above with $g_{a\gamma\gamma} < 10^{-10}$ GeV^{-1} by the number of horizontal branch stars in globular clusters. KSVZ [46, 47] and DFSZ [8, 9] are two different theoretical models that predict how $g_{a\gamma\gamma}$ scales with m_a. Other exclusion regions are from lab experiments by the CAST experiment [14], ADMX group [15, 16] and by Rochester-Brookhaven-Fermilab collaboration [17, 18] (color online).

Naively, one would expect the plane of polarization to rotate by an amount that is $\mathcal{O}(g_{a\gamma\gamma}^2 B^2 l^2)$, which is valid strictly in the absence of plasma when the photon and axion are treated as massless particles [20, 44]. Therefore, for a fixed degree of polarization an increase in B should also decrease $g_{a\gamma\gamma}$ by the same factor, when l, the length over which the magnetic field remains homogeneous, is kept constant. However, as shown by [45] in the case of NSs, an increase in magnetic field strength also increases the level of polarization by effectively shifting the polarization-limiting radius, the distance beyond which the two polarization modes couple and which depends weakly on the magnetic field strength $R_{pl} \propto B^{2/5}$, farther away from the star. The farther the polarization-limiting radius, the more coherently the polarization states from different LOSs add, yielding a higher degree of polarization.

IV. DISCUSSION

This study looks at how the production of axions in mWD magnetospheres can alter the state of polarization of the observed radiation. We find that unpolarized photons of photospheric origin become linearly polarized upon their traversal through the inhomogeneous magnetic field of a mWD. We have modeled the magnetospheric plasma, as fully ionized pure H with a barometric profile. Since the majority of mWDs are strongly circularly polarized and only show a relatively small degree of linear polarization, at most 5%, we have used this observation to constrain the coupling strength $g_{a\gamma\gamma}$ of axions to photons. We find that for the case where the plasma component only contributes negligibly to the state of polarization, the coupling strength $g_{a\gamma\gamma}$ increases with the mass of the axion m_a. The level of linear and circular polarization observed in mWDs is sensitive to the properties of the magnetospheric plasma. The limits on $g_{a\gamma\gamma}$ can be improved by modelling all the radiative transfer effects in WD atmospheres and fitting the model spectra to real observations.

Magnetic fields stronger than that of mWDs exist in NSs. Going back to the argument of how astrophysical objects, compared to laboratory experiments, benefit from longer coherence lengths (see Section I), in comparing mWDs with NSs, one finds that the latter are $\sim 10^4$ times more efficient in converting photons to axions and vice-versa. A number of studies have expounded on the subject of propagation of polarized radiation through the NS magnetosphere, where they have considered IR/Optical radiation [48], and thermal X-rays [32, 49] produced at the surface of the NS. Unfortunately, no X-ray polarimetry observations have been conducted partly due to the very low flux in X-rays from these objects, and also because none of the high energy telescopes are equipped with a polarimeter. X-ray polarimetry has been neglected for the last 30 years but it is hoped that some of the future space missions [50], for example the Gravity and Extreme Magnetism Small Explorer (GEMS) [51], will fill this void in X-ray astronomy. In any case, as discussed by [19–21], NSs are excellent laboratories for the detection of any light, weakly coupled pseudoscalar particle.

A. Outlook

The ADMX[3] project, that employs a microwave cavity to search for cold dark matter axions, will begin its phase II of testing in the year 2012. With the new upgrades the ADMX project will be able to exclude $g_{a\gamma\gamma}$ up to the DFSZ line in the same mass range as before. Although outside of the range of axion masses probed in

[3] http://www.phys.washington.edu/groups/admx/experiment.html

this study, the modified CAST experiment has been able to exclude axions with $g_{a\gamma\gamma} \gtrsim 2.2 \times 10^{-10}$ GeV^{-1} for $m_a \lesssim 0.4$ eV, becoming the first experiment to ever cross the KSVZ line [52, 53]. The currently running CAST experiment in its phase-II will be able to exclude axions with $m_a \lesssim 1.15$ eV with unprecedented sensitiviy in this mass range. An improved version of the *light shining through wall* (LSW) experiment ([44], also see [54] for a recent review on such experiments) using Fabry-Perot optical cavities to resonantly enhance photon-axion conversion has been proposed [55–57]. The projected limit in sensitivity to $g_{a\gamma\gamma} \gtrsim 2.0 \times 10^{-11}$ GeV^{-1} typically for axion masses $m_a \lesssim 10^{-4}$ eV achieved using 12 Tevatron superconducting dipoles appears quite promising. Further improvements in experiment design and optimization techniques yielding increased sensitivity to even smaller coupling strengths have also been suggested by many workers in the field, for example the use of the dipole magnets, each providing a field strength of 5 T, from the Hadron Electron Ring Accelerator (HERA) at DESY in Hamburg in a 20+20 configuration can potentially exclude $g_{a\gamma\gamma} \gtrsim 10^{-11}$ GeV^{-1} for $m_a < 10^{-4}$ eV [58, 59]. Another proposed line of investigation to search for axion like particles (ALPs) is the use of resonant microwave cavities which are much similar in design to the optical LSW experiments discussed above [60–62]. This method has already been employed to search for hidden sector photons [63] and can prove to be a powerful tool in the case of axions.

Finally, the simplistic model assumed for the mWD atmosphere only yields an absolute upper bound on $g_{a\gamma\gamma}$. A much tighter constraint can be obtained by adopting a more realistic atmospheric model and solving the equations of radiative transfer with the photon-axion oscillations included. Such an analysis is outside the scope of this study, but it is hoped that the novel method discussed in this work will prove to be extremely useful in better constraining the properties of any ALP.

ACKNOWLEDGMENTS

We would like to thank the referee for significantly improving the quality of this work. R.G. acknowledges support by the NSERC CGS-D3 scholarship. The Natural Sciences and Engineering Research Council of Canada, Canadian Foundation for Innovation and the British Columbia Knowledge Development Fund supported this work. Correspondence and requests for materials should be addressed to J.S.H. (heyl@phas.ubc.ca). This research has made use of NASAs Astrophysics Data System Bibliographic Services

[1] J. E. Kim and G. Carosi, Reviews of Modern Physics **82**, 557 (2010).
[2] F. Wilczek, Physical Review Letters **40**, 279 (1978).
[3] V. Baluni, Phys. Rev. D**19**, 2227 (1979).
[4] C. A. Baker *et al.*, Physical Review Letters **97**, 131801 (2006).
[5] R. D. Peccei and H. R. Quinn, Physical Review Letters **38**, 1440 (1977).
[6] S. Weinberg, Physical Review Letters **40**, 223 (1978).
[7] J. Preskill, M. B. Wise, and F. Wilczek, Physics Letters B **120**, 127 (1983).
[8] M. Dine, W. Fischler, and M. Srednicki, Physics Letters B **104**, 199 (1981).
[9] A. Zhitnitskii, Sov. J. Nucl. Phys. **31**, 260 (1980).
[10] G. G. Raffelt, Physics Letters B **592**, 391 (2004).
[11] G. G. Raffelt, *Stars as laboratories for fundamental physics : the astrophysics of neutrinos, axions, and other weakly interacting particles* (University of Chicago Press, Chicago, 1996).
[12] G. G. Raffelt, Annual Review of Nuclear and Particle Science **49**, 163 (1999).
[13] S. J. Asztalos *et al.*, Annual Review of Nuclear and Particle Science **56**, 293 (2006).
[14] S. Andriamonje *et al.*, J. Cosmology Astropart. Phys.**4**, 10 (2007).
[15] S. J. Asztalos *et al.*, Phys. Rev. D**69**, 011101 (2004).
[16] S. J. Asztalos *et al.*, Physical Review Letters **104**, 041301 (2010).
[17] S. De Panfilis *et al.*, Physical Review Letters **59**, 839 (1987).
[18] W. U. Wuensch *et al.*, Phys. Rev. D**40**, 3153 (1989).
[19] D. Chelouche, R. Rabadán, S. S. Pavlov, and F. Castejón, ApJS**180**, 1 (2009).
[20] G. Raffelt and L. Stodolsky, Phys. Rev. D**37**, 1237 (1988).
[21] D. Lai and J. Heyl, Phys. Rev. D**74**, 123003 (2006).
[22] M. S. Pshirkov and S. B. Popov, Soviet Journal of Experimental and Theoretical Physics **108**, 384 (2009).
[23] R. Jimenez, C. Pena-Garay, and L. Verde, ArXiv:1102.1728 (2011).
[24] J. C. Kemp, J. B. Swedlund, J. D. Landstreet, and J. R. P. Angel, ApJ**161**, L77+ (1970).
[25] D. T. Wickramasinghe and L. Ferrario, PASP**112**, 873 (2000).
[26] F. Euchner *et al.*, A&A**390**, 633 (2002).
[27] J. C. Kemp, ApJ**162**, 169 (1970).
[28] J. R. P. Angel, ApJ**216**, 1 (1977).
[29] V. N. Sazonov and V. V. Chernomordik, Ap&SS**32**, 355 (1975).
[30] F. Euchner *et al.*, A&A**451**, 671 (2006).
[31] P. Meszaros and J. Ventura, Phys. Rev. D**19**, 3565 (1979).
[32] D. Lai and W. C. G. Ho, ApJ**588**, 962 (2003).
[33] W. H. Ingham, K. Brecher, and I. Wasserman, ApJ**207**, 518 (1976).
[34] V. V. Zheleznyakov and A. V. Serber, Space Sci. Rev.**68**, 275 (1994).
[35] T. A. Fleming *et al.*, A&A**316**, 147 (1996).
[36] Z. E. Musielak, M. Noble, J. G. Porter, and D. E. Winget, ApJ**593**, 481 (2003).
[37] A. Dupays and M. Roncadelli, arXiv:astro-ph/0612176 (2006).

[38] G. B. Rybicki and A. P. Lightman, *Radiative processes in astrophysics* (WILEY-VCH, Verlag GmbH & Co., KGaA, Weinheim, 2004).
[39] S. P. Mikheev and A. Y. Smirnov, Sov. J. Nucl. Phys. **42**, 913 (1985).
[40] L. Wolfenstein, Phys. Rev. D**17**, 2369 (1978).
[41] S. Jordan, in *IAU Symposium*, Vol. 259 of *IAU Symposium* (Cambridge University Press, Cambridge, UK, 2009), pp. 369–378.
[42] V. Piirola and A. Reiz, A&A**259**, 143 (1992).
[43] K. M. Vanlandingham *et al.*, AJ**130**, 734 (2005).
[44] K. van Bibber *et al.*, Physical Review Letters **59**, 759 (1987).
[45] J. S. Heyl, N. J. Shaviv, and D. Lloyd, MNRAS**342**, 134 (2003).
[46] J. E. Kim, Physical Review Letters **43**, 103 (1979).
[47] M. A. Shifman, A. I. Vainshtein, and V. I. Zakharov, Nuclear Physics B **166**, 493 (1980).
[48] R. M. Shannon and J. S. Heyl, MNRAS**368**, 1377 (2006).
[49] D. Lai and W. C. Ho, Physical Review Letters **91**, 071101 (2003).
[50] F. Muleri *et al.*, Mem. Soc. Astron. Italiana**81**, 488 (2010).
[51] K. Jahoda, in *Society of Photo-Optical Instrumentation Engineers (SPIE) Conference Series* (SPIE publications, Bellingham, WA, 2010), Vol. 7732.
[52] E. Arik *et al.*, J. Cosmology Astropart. Phys.**2**, 8 (2009).
[53] S. Aune *et al.*, ArXiv:1106.3919 (2011).
[54] J. Redondo and A. Ringwald, Contemporary Physics **52**, 211 (2011).
[55] F. Hoogeveen and T. Ziegenhagen, Nuclear Physics B **358**, 3 (1991).
[56] G. Mueller, P. Sikivie, D. B. Tanner, and K. van Bibber, Phys. Rev. D**80**, 072004 (2009).
[57] P. Sikivie, D. B. Tanner, and K. van Bibber, Physical Review Letters **98**, 172002 (2007).
[58] A. Ringwald, Physics Letters B **569**, 51 (2003).
[59] P. Arias, J. Jaeckel, J. Redondo, and A. Ringwald, Phys. Rev. D**82**, 115018 (2010).
[60] F. Hoogeveen, Physics Letters B **288**, 195 (1992).
[61] F. Caspers, J. Jaeckel, and A. Ringwald, Journal of Instrumentation **41**, 11013 (2009).
[62] J. Jaeckel and A. Ringwald, Physics Letters B **659**, 509 (2008).
[63] R. G. Povey, J. G. Hartnett, and M. E. Tobar, Phys. Rev. D**82**, 052003 (2010).